energies

MDPI

Article

Thermoeconomic Optimization Design of the ORC System Installed on a Light-Duty Vehicle for Waste Heat Recovery from Exhaust Heat

Xialai Wu [1], Ning Zhang [1], Lei Xie [2], Wenyan Ci [1], Junghui Chen [3,*] and Shan Lu [4,*]

[1] School of Engineering, Huzhou University, Huzhou 313000, China; wxlai@zjhu.edu.cn (X.W.); hzu0732@126.com (N.Z.); ciwenyan@zjhu.edu.cn (W.C.)
[2] State Key Laboratory of Industrial Control Technology, Zhejiang University, Hangzhou 310027, China; lxie@zju.edu.cn
[3] Department of Chemical Engineering, Chung-Yuan Christian University, Chung-Li, Taoyuan 320, Taiwan
[4] Institute of Intelligence Science and Engineering, Shenzhen Polytechnic, Shenzhen 518055, China
* Correspondence: jason@wavenet.cycu.edu.tw (J.C.); lushan@spzt.edu.cn (S.L.)

Abstract: The organic Rankine cycle (ORC) has been widely studied to recover waste heat from internal combustion engines in commercial on-road vehicles. To achieve a cost-effective ORC, a trade-off between factors such as costs, power outputs, back pressure, and weight needs to be carefully worked out. However, the trade-off is still a huge challenge in engine waste heat recovery. In this study, a thermoeconomic optimization study of a vehicle-mounted ORC unit is proposed to recover waste heat from various exhaust gas conditions of a light-duty vehicle. The optimization is carried out for four organic working fluids with different critical temperatures, respectively. Under the investigated working fluids, the lower specific investment cost (SIC) and higher mean net output power (MEOP) of ORC can be achieved using the organic working fluid with higher critical temperature. The maximum mean net output power is obtained by taking RC490 as working fluid and the payback period (PB) is 3.01 years when the petrol is EUR 1.5 per liter. The proposed strategy is compared with a thermodynamic optimization method with MEOP as an optimized objective. It shows that the proposed strategy reached SIC results more economically. The importance of taking the ORC weight and the back pressure caused by ORC installation into consideration during the preliminary design phase is highlighted.

Keywords: ORC design; thermoeconomic optimization; vehicle exhaust heat recovery

Citation: Wu, X.; Zhang, N.; Xie, L.; Ci, W.; Chen, J.; Lu, S. Thermoeconomic Optimization Design of the ORC System Installed on a Light-Duty Vehicle for Waste Heat Recovery from Exhaust Heat. *Energies* **2022**, *15*, 4486. https://doi.org/10.3390/en15124486

Academic Editor: Andrea De Pascale

Received: 30 April 2022
Accepted: 17 June 2022
Published: 20 June 2022

1. Introduction

Currently, it is difficult to further improve the thermal efficiency of an internal combustion engine (ICE) technically [1]. More than 50% of the fuel energy released in an ICE is discharged into the environment as waste heat, in which a large part of energy is wasted in the form of exhaust gas [2]. It was reported that a potential fuel consumption improvement of around 10% for ICE would be obtained if 6% of the heat in exhaust gas can be recovered and converted into useful mechanical power [3,4]. In the literature, the waste exhaust heat can be recovered through turbo-compounding [5], thermofluidic oscillators [6], thermoelectric generators [7], organic Rankine cycle (ORC) [8,9], etc. Among the aforementioned methods of the ICEs waste heat recovery, the ORC is a widely studied and well-recognized method because of its simple configuration, high waste heat utilization, and reliability [10,11].

The application of ORC in vehicle ICE waste heat recovery to generate a power output for economic and environmental benefits has attracted widespread interest. To improve the ORC performance, working fluid selection [12], the architecture of the cycle [13], controller design [14], etc., have already been investigated in the literature. However, due to the contradiction between ORC's thermodynamic performance and costs, it is not easy to design a high-performance and economical ORC. Particularly, the additional weight, back pressure, and cooling demand caused by ORC installation on a vehicle are three factors that would greatly decrease the benefits of ORC applications on waste heat recovery of ICEs. Therefore, a trade-off among the factors such as thermodynamic performance, costs, and weight needs to be performed during the preliminary design procedure of onboard ORC units.

In the literature, the most suitable way to design a good ORC system is to carry out an optimization problem with a suitable objective. Valencia et al. [15] performed thermoeconomic optimizations of a double-loop ORC integrated into a 2 MW natural gas engine using toluene as the working fluid. The operating parameters, such as evaporation pressures, pinch-point temperatures of exchangers, etc., were optimized to maximize the ORC's net output power and to minimize the payback period, specific investment cost (SIC), and levelized costs of energy. However, the optimization of the ORC system was only conducted in one exhaust condition, so the off-design performance of the ORC designed cannot be guaranteed. Li et al. [16] conducted an optimization based on a thermoeconomic indicator for a small-scale dual-pressure evaporation ORC system. The effects of the heat source conditions on the economic performance of the system were investigated. However, the various heat source conditions were not simultaneously taken into account during the design procedure, so the off-design performance and feasibility of ORC were still not guaranteed. Imran et al. [9] carried out optimization of ORC mounted on the heavy-duty vehicles using the sizing and technoeconomic indicators, and the off-design performances of designed ORC were also evaluated for a real driving cycle. However, the extra condensing consumption was not considered. A multi-objective optimization of double-loop ORC (DORC) was carried out by Ping et al. for a compressed natural gas engine [17]. The operating parameters were optimized to improve the thermoeconomic and environmental performance of DORC, but the negative factors, such as the back pressure imposed by the ORC unit installation, were not considered. Wu et al. proposed an ORC optimization method considering various major exhaust conditions of a light-duty vehicle and the negative effects of ORC weight and back pressure [8]. The results highlighted the necessity of taking the multiple main exhaust conditions and the negative effects into account during the optimization design of ORC. However, the economic performance, such as the total investment cost, was not included in the optimization problem. A list of ORC optimization studies for recovering waste heat from ICEs are summarized in Table 1.

The literature review shows that investigation of the optimization of the ORC system applied in ICE waste heat recovery has been widely conducted. However, a thermoeconomic optimization design of the onboard ORC system considering multiple exhaust gas conditions and the negative impacts of ORC application has not been presented. To design a high-performance and cost-effective ORC for exhaust heat recovery from a light-duty vehicle, this paper proposes an overall thermoeconomic optimization method for the vehicle-mounted ORC. The negative impacts of the ORC application on the light-duty vehicle and the multiple exhaust conditions are taken into account during the optimization. The negative impacts are quantified, respectively, in the form of the additional ICE power consumption. The optimization is performed for four different working fluids using a specific investment cost (SIC) as an objective. Furthermore, the proposed optimization methodology is compared with the optimization strategy using mean net output power as an objective. The details are presented as follows: In Section 2, the schematic of the onboard ORC unit is provided. Section 3 presents the thermoeconomic model and optimization methodology. The optimization results and comparison between the two optimization strategies are discussed in Section 4. At last, the conclusions are given in Section 5.

Table 1. The optimization studies of ORC applied to waste heat recovery of ICEs. OP represents the operating parameters, GP represents the geometric parameters, LCOE is the levelized cost of energy, ECE is the emissions of CO_2 equivalent, ΔT_{exch} is the pinch-point temperature difference of a heat exchanger, and Var_{η} is the variance of thermal efficiency.

Ref.	Objective Functions			Decision Variables	Number of Exhaust Condition	Cooling Consumption	Negative Factors
	Economic	Thermal	Others				
[8]	-	$\dot{W}_{net}$	-	OP, GP	Multi	-	TM, ΔP_{bp}
[9]	TIC	$\dot{W}_{net}$	TV, TM	OP	One	-	TV, TM, ΔP_{bp}
[18]	TIC	$\dot{W}_{net}$	-	OP	Multi	-	-
[15]	PB, SIC	$\dot{W}_{net}$	LCOE	OP	One	-	-
[19]	PB	η_e	-	OP, ΔT_{exch}	One	-	-
[20]	TIC	$\dot{W}_{net}$	-	OP	One	-	-
[21]	SIC		VC, A_{tol}	OP	One	-	-
[22]	TIC_{yr}	η_{th}	-	OP, $\dot{W}_{Eng}$, $\dot{W}_{Eng,pl}$	-	-	-
[23]	PB	η_e	-	OP	One	-	-
[24]	TIC	$\dot{W}_{net}$	-	OP	Multi	-	-
[16]	SIC		-	OP	Multi	$\dot{W}_c$	-
[25]	SIC		-	OP	Multi	-	TM, ΔP_{bp}
[26]	-	η_{th}, Var_{η}	-	OP, ΔT_{exch}	One	-	-
[27]	-	$\dot{W}_{exp}$	-	OP	One	-	-
[17]	PB	η_{th}	ECE	OP	One	-	-
[28]	-	η_{Conv}	-	OP	One	$\dot{W}_c$	-

2. Onboard ORC System and Optimization Methodology

2.1. System Description

The schematic of onboard ORC is presented in Figure 1. The different thermodynamic states of the working fluid in the two heat exchangers are represented by points 1–8, and the state points 9–16 represent the actual changes of the exhaust gas and cooling air. These state points will be used for modeling in Section 3.1. The cooling air temperature in this paper is assumed to always be 25 °C, and the isentropic efficiencies of the pump and expander are assumed to be 0.4 and 0.65, respectively, for simplicity. Both isentropic efficiencies are chosen based on the published papers, which show that the isentropic efficiency of the pump and expander are, respectively, in the ranges of 7% to 60% [29–31] and 26% to 73.4% [29,32,33].

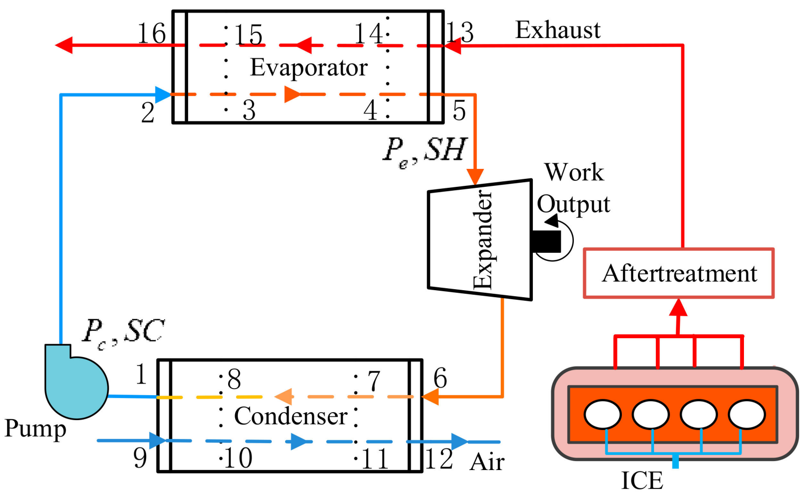

Figure 1. The schematic of the onboard ORC system in this work.

The selection of working fluids for waste heat recovery based on ORC has been investigated by numerous studies [24,34,35]. In this paper, our work focuses on proposing an ORC thermal–economic optimization method that considers the negative impact of the ORC installation and validates the obtained optimization results under drastic changes in exhaust heat conditions of a light-duty vehicle. To study the effect of working fluids with different critical temperatures on the results of thermal–economic optimization, four working fluids with different critical temperatures were selected from the available literature [32,33] and are listed in Table 2.

Table 2. The thermophysical properties of the four working fluids.

Fluid	Critical Temperature T_{cr} (°C)	Molar Mass (kg/kmol)	Normal Boiling Point (°C)	Critical Pressure P_{cr} (MPa)	Latent Heat (kJ/kg) [a]
R245fa	154.1	134.0	15.1	3.6	91.7
R245ca	174.4	134.0	25.1	3.9	95.7
R601a	187.2	72.1	27.8	3.4	151.7
RC490	238.6	70.1	49.2	4.5	212.9

[a] At the evaporation pressure of 2.5 MPa.

In general, the category of working fluid affects the design of an ORC [34]. If the sensible heat after the expansion of the working fluid is reused through the recuperator, the heat load of the condenser decreases, and correspondingly, the condensation consumption of the condenser is reduced. However, since the ORC is applied to the vehicle, the use of the recuperator will increase the total amount of ORC, and this added weight will consume power from the vehicle's engine, which may offset the benefits of using the recuperator. At the same time, the use of the recuperator also increases the cost. Furthermore, since the working conditions of the vehicle exhaust gas (the temperature and the mass flowrate) change drastically, the operation of the ORC system needs to be controlled, so the addition of a recuperator increases the system complexity and brings challenges to control. Therefore, the simple ORC used in this study for vehicle waste heat recovery is a viable option [25,35].

The exhaust gas data (temperatures and mass flow rates of the exhaust gas measured from a light-duty vehicle mounted with a 2.8 L VR6 spark ignition engine) are provided in Ref. [36]. The weight of the reference vehicle is 1340 kg. The exhaust measurement data at five major operating points of the engine are presented in Table 3. A percentage factor is assigned to each engine operating point, as shown in the rightmost column of Table 3. It represents the percentage of time at each operating point during engine operation [8]. A well-designed ORC should be able to work in different exhaust conditions through the adjustment of ORC operating conditions. Therefore, five major exhaust conditions in Table 3 will be fully considered during the optimal design of the ORC unit in this paper.

Table 3. Exhaust conditions and percentage factors at five major engine operating points.

Engine Operating Point	Mass Flow Rate of Exhaust (g/s)	Temperature of Exhaust (°C)	Engine Power (kW)	Vehicle Speed (km/h)	Percentage Factor (%)
1	25.9	595.1	13.0	23.5	5.0
2	43.0	716.7	26.4	47.2	8.1
3	59.7	779.2	37.2	67	16.9
4	71.9	800.7	44.1	80	31.3
5	92.4	804.1	54.4	100	36.6

The evaporator and the condenser in the ORC system are brazed plate heat exchangers with a chevron angle of 45°. The constant geometric parameters of the plate heat exchanger listed in Table 4 are obtained based on several papers [21,37,38]. The number of heat exchange plates (N_p) and the length of the plate (L_p) are the variable geometric parameters used to determine the size of the plate heat exchanger. These free parameters will be optimized to obtain compact heat exchangers with reasonable costs to meet the heat exchange requirements.

Table 4. The constant geometric parameters of the plate heat exchanger.

Parameter	Value
Width of plate (W_p)	0.1 m
Chevron angle ($\beta_{chevron}$)	45°
Thermal conductivity (k_p)	14.9 W/m·K
Hydraulic diameter (D_h)	2 mm
Plate thickness (d_p)	0.002 m

2.2. Thermoeconomic Optimization

ORC is an auxiliary system for the vehicle to realize the waste heat recovery of the engine, and its economy is a key concern. To obtain a cost-effective ORC with high thermodynamic performance, an optimization with a thermoeconomic indicator (i.e., SIC) is performed in this study. The three negative factors (additional weight, back pressure, and cooling demand) caused by ORC installation on a vehicle are comprehensively considered in the optimization process. In addition, the various exhaust gas conditions in Table 3 are taken into account for the optimal design of the ORC system. The thermoeconomic optimization problem for the ORC design is formulated as follows.

$$\begin{aligned} &\min_{[\mathbf{v}_d,\mathbf{v}_c]} \ \mathrm{SIC} = \frac{Cost_{ORC}}{\overline{\dot{W}}_{net}} \\ &s.t. \\ &\qquad ORC\ models \\ &\qquad system\ constraints \end{aligned} \tag{1}$$

where $\overline{\dot{W}}_{net} = \sum_{i=1}^{N_{ex}} w_i \dot{W}_{net,i}$ is the weighted average net output power, N_{ex} is the number of exhaust conditions, w_i is the percentage factor, and $\dot{W}_{net,i}$ is the ORC system's net output power in the i-th exhaust condition. Because of ORC installation, the cooling power consumption and the additional engine power consumption are taken into account in the net output power calculation. The vector of optimized geometric parameters in heat exchangers is

$$\mathbf{v}_d = \left[N_{pe}, L_{pe}, N_{pc}, L_{pc}\right]$$

The optimized operating parameters of the ORC system corresponding to N_{ex} different exhaust conditions are expressed as

$$\mathbf{v}_c = [P_{e1}, SH_{e1}, P_{c1}, SC_{c1}, \cdots, P_{eN_{ex}}, SH_{eN_{ex}}, P_{cN_{ex}}, SC_{cN_{ex}}]$$

The evaporating pressure (P_e), condensing pressure (P_c), superheat (SH), and subcooling (SC) are often selected as operating parameters in the ORC system. Changing these operating parameters will change the net output power of the ORC system and then affect the objective (SIC) of the proposed optimization problem. The sensitivity analysis of the SIC is carried out by varying the operating parameters at one exhaust condition (800.7 °C, 71.9 g/s). The working fluid is R245ca, and the results are shown in Figure 2. It can be found that the SIC varies with the change of each operating parameter.

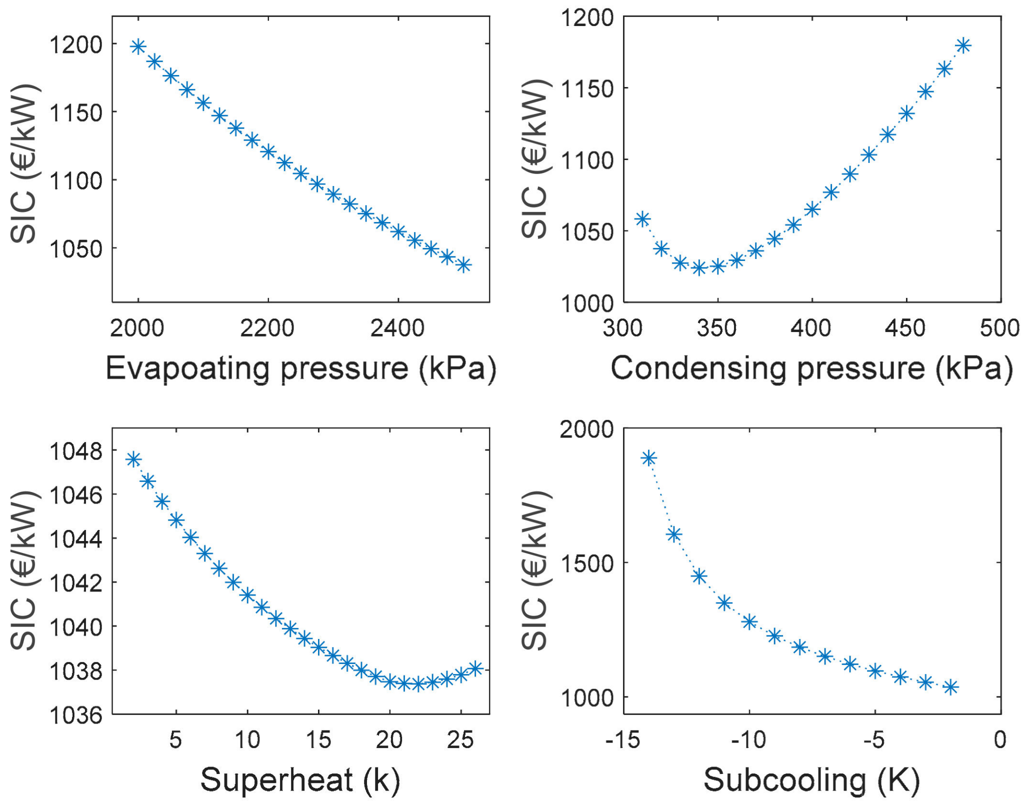

Figure 2. Impact of the operating parameters on the optimization objective (SIC).

In this study, SIC is adopted as the optimization objective to maximize the mean net output power and minimize the investment cost of the onboard ORC system. The trade-offs between the thermodynamic performance and the cost are performed by the optimization to obtain the optimum design parameters for each major exhaust condition. To calculate the objective value, the thermodynamic model, cost model, and weight model of the ORC system are all involved in the optimization problem. These models will be explained more in Section 3.

To ensure the safe operation of a vehicle-mounted ORC, some safety constraints are imposed in the optimization problem:

1. To avoid corrosion damage to the heat exchanger, the outlet exhaust gas temperature is maintained at above 130 °C in this study, which is above the acid dew point.
2. The working fluid temperature in ORC is kept below its critical temperature based on the reference [30,36]. This setting avoids decomposition and chemical deterioration of the organic working fluid because of the high temperature.
3. Since the conditions of the vehicle exhaust gas (the temperature and the mass flowrate) change drastically, the superheat of the working fluid is maintained positive to ensure working fluid entering the expander is dry, which prevents the occurrence of the liquid strike in the expander, and eases the difficulty of control design. It should be greater than 2 K in this study to ensure that the working fluid is dry vapor in the expander even though the heat losses happen in practice.
4. To avoid the working fluid vaporization in the pump, a certain amount of subcooling is required at the pump inlet. The subcooling is set to be greater than 2 K in this study.

Considering the thermophysical properties of the working fluids and the actual limitation of the equipment, such as mechanical strength of the equipment materials, the upper and lower limits of the decision variables were selected and are given in Table 5.

Table 5. The optimization range of the decision variables.

Variables	Description	Ranges
P_e	Evaporating pressure, (kPa)	[1800, 2500]
P_c	Condensing pressure, (kPa)	[300, 500]
SH	Superheating, (K)	[2, 30]
SC	Subcooling, (K)	[2, 10]
L_{pe}	Plate length in the evaporator, (m)	[0.4, 0.6]
L_{pc}	Plate length in the condenser, (m)	[0.4, 0.6]
N_{pc}	The number of condensing plates	[45, 200]
N_{pe}	The number of evaporating plates	[20, 86]

3. Models

The whole thermoeconomic ORC model is built and implemented in MATLAB (R2020a) in combination with the REFPROP library. The REFPROP library is used for the calculation of the thermodynamic properties of organic fluids. The framework consists of a steady-state ORC thermodynamic model, plate heat exchanger models, and correlations to estimate the capital costs and mass of the ORC components.

3.1. The ORC Model

In the cycle thermodynamic description, the thermal equilibrium equations of the ORC components are described based on our previous work [8]. The thermodynamic calculations for each component with state points in Figure 1 are expressed and listed in Table 6.

Table 6. The thermodynamic calculations for each component of the ORC system.

Process (State Points)	Component	Thermodynamic Equations
1-2	Pump	$\dot{W}_p = \dot{m}_f(h_2 - h_1)$ $h_2 = h_1 + \frac{(h_{2s} - h_1)}{\eta_{is,p}}$
2-3-4-5, 13-14-15-16	Evaporator	$\dot{Q}_e = \dot{m}_f(h_5 - h_2) = \dot{m}_{exh}(h_{13} - h_{16})$
5-6	Expander	$\dot{W}_{\exp} = \dot{m}_f(h_5 - h_6)$ $h_6 = h_5 - (h_5 - h_{6s})\eta_{is,\exp}$
6-7-8-1, 9-10-11-12	Condenser	$\dot{Q}_c = \dot{m}_f(h_6 - h_1) = \dot{m}_{air}(h_{12} - h_9)$

To account for the negative impacts caused by the ORC installation, the net power output ($\dot{W}_{net}$) of the onboard ORC system is defined as

$$\dot{W}_{net} = \dot{W}_{\exp} - \dot{W}_p - \dot{W}_A - \dot{W}_{backp} - \dot{W}_{orc,w} \quad (2)$$

Where $\dot{W}_A = \dot{m}_{air}\mu_A$, μ_A is the coefficient of power consumption, and $\dot{W}_{backp}$ and $\dot{W}_{orc,w}$, which will be detailed in Section 3.4, are the power losses caused by back pressure and weight, respectively.

3.2. Model of the Heat Exchanger

The heat exchanger has a great impact on the system efficiency and economics. Since the geometric parameters, including the length of the heat exchanging plate and the number of plates, are taken as the decision variables of the formulated thermoeconomic optimization, an integrated model of the heat exchanger combining a thermodynamic and a geometric model is proposed. The heat transfer model of the plate heat exchanger is established using the log-mean temperature difference (LMTD) method, which is based on counter-flow heat exchangers [8,19]. According to the three different phases of working fluid experiences during heat exchange, the heat exchanger is subdivided into three movingboundary zones, including a subcooling zone, a two-phase zone, and a superheat zone. The heat transfer area (A_i) corresponding to each zone can be expressed as

$$A_i = \frac{\dot{Q}_i}{U_i \Delta T_{LM,i}} \text{ with } i = 1, 2, 3 \tag{3}$$

where $\dot{Q}_i$ is the heat flow rate of the ith zone (in W), $\Delta T_{LM,i}$ denotes the LMTD between the hot fluid and the cold fluid (in K) in the ith zone, and U_i is the overall heat transfer coefficient (in W/(m^2 K)).

After the area of each zone is calculated, the total heat transfer area of the heat exchanger (A_{Ltol}) can obviously be derived by summing as follows:

$$A_{Ltol} = \sum_{i=1}^{3} A_i \tag{4}$$

3.2.1. Heat Transfer Coefficients and Pressure Drops

The heat source and sink stream (i.e., exhaust gas and cooling air in this study) do not undergo phase change; they remain gaseous during the ORC operation. Furthermore, the working fluid in the subcooling zone and superheat zone is present as a single-phase liquid and a single-phase vapor, respectively. The heat transfer coefficients (h) in these single-phase zones of the evaporator and the condenser are determined by the Thonon correlation [21]. The working fluid in the two-phase zone undergoes a phase transition, and the evaporating heat transfer coefficient of the surface is taken from Hsieh and Lin's studies [39,40] while the condensing heat transfer coefficient is predicted using the Kuo correlation [41]. Table 7 shows the correlations of the heat transfer coefficient in the heat exchangers. In Table 7, P_r is the Prandtl number, λ is the fluid thermal conductivity, R_e is the Reynolds number, calculated by the fluid thermal properties, D_h is the hydraulic diameter, C_n and S are the correlation constants, B_O is the boiling number, Fr_l is the Froude number in saturated liquid state, g is the acceleration due to gravity, and x and C_O are the vapor quality and the convection number, respectively.

Table 7. Heat-transfer coefficient equations for heat exchangers.

		Correlations
Single-phase	[16]	$h = \frac{\lambda}{D_h} C_n R_e{}^s P_r{}^{\frac{1}{3}}$
Two-phase	Boiling process [39]	$h_{tp,e} = 88 \cdot h_{liq} \cdot B_O{}^{0.5}$
	Condensing process [41]	$h_{tp,c} = h_{liq}\left(0.25 C_O{}^{-0.45} Fr_l{}^{0.25} + 75 B_O{}^{0.75}\right)$
		$C_O = \frac{\rho_v}{\rho_l}\left(\frac{1}{x} - 1\right)^{0.8}$, $Fr_l = \frac{G^2}{\rho_l{}^2 g D_h}$

Since the flows in the channels of the plate heat exchanger are assumed to be horizontal, the pressure drop due to gravity and elevation is neglected. The channel single-phase frictional pressure drop is computed by [37]

$$\Delta p_f = \frac{2 f \rho u^2 L_{eff} N_{pass}}{D_h} \left(\frac{\mu}{\mu_w}\right)^{0.17} \tag{5}$$

where μ is the fluid viscosity, μ_w is the fluid viscosity in the temperature of the channel wall, N_{pass} is the number of passes, u is the fluid velocity, and L_{eff} is the effective length of the fluid flow path between the inlet and outlet ports. f is the friction factor that is computed by

$$f = \frac{K_p}{R_e^m} \tag{6}$$

where K_p and m are correlation constants depending on the chevron angle $\beta_{chevron}$ and R_e ($\beta_{chevron} = 45°$ is used in this study).

The pressure drop of the port ducts is computed by the relation [8]

$$\Delta p_p = 1.4 N_{pass} \rho \frac{u_p^2}{2} \tag{7}$$

where u_p is the port velocity of the working fluid, and ρ is the fluid density.

The total pressure drop in the hot side of the evaporator is computed by the summation of the frictional pressure drop Δp_f and the port pressure drop Δp_p. Since the evaporation pressure and condensing pressure are much higher than the pressure drop, the pressure drop in the working fluid side is neglected in this study.

3.2.2. Model Calculation of the Plate Heat Exchanger

As the plate heat exchanger is composed of plates, the total heat transfer area of the heat exchanger varies depending on the number of those plates and the plate geometric parameters. The total heat transfer area can be computed by

$$A_{Gtol} = \left(N_p - 2\right) \times L_p \times W_p \tag{8}$$

where W_p is the effective plate width.

During the calculation of the combined heat exchanger model, the total heat transfer area (A_{Gtol}) computed by geometric parameters with Equation (8) needs to be equal to the total heat transfer area (A_{Ltol}) obtained by means of the LMTD method in Equation (4). Hence, the calculation process of the heat exchanger model is iterative.

For simplicity, only the calculation of the evaporator model is illustrated, and the flow chart is presented in Figure 3. The inlet conditions of the exhaust (the secondary fluid in the exchanger except for the working fluid), evaporator geometric parameters, and the operating parameters (such as evaporating pressure and superheat) are taken as inputs for the evaporator model calculation. Initially, the exhaust exit temperature ($T_{exh,o}$) is assumed and the resulting total heat transfer area (A_{Ltol}) in the evaporator is obtained by the LMTD method. The iterative calculation process continues by means of the changing exhaust exit temperature until the corresponding total area is equal to the total heat transfer area (A_{Gtol}) obtained by the evaporator geometric parameters.

3.3. Economic Model

Investment costs are one of the main issues concerned when the ORC system is applied to the waste heat recovery from the vehicle exhaust gas. It is necessary to evaluate the cost of the ORC unit during the preliminary design of the ORC system. In Table 8, the cost correlations of the main components in the ORC system are adopted from the available papers [9,21,37,42].

Table 8. Cost correlations for the main components of ORC [9,21,37,42].

Component	Dependent Variable	Correlation Equation (€)
Expander	Volume flow rate, $\dot{V}_{in}$ (m^3/s)	$C_{exp} = 21.556 V_d^{0.6271}$
Pump	Pump power, $\dot{W}_p$ (W)	$C_p = 150 * \left(\dot{W}_p/300\right)^{0.25}$
Plate heat exchanger	Heat exchange area, A_{Ltol} (m^2)	$C_{hx} = 190 + 310 * A_{Ltol}$

The cost of each component in the cycle is used to estimate the total ORC investment cost ($Cost_{ORC}$), and it is presented as follows.

$$Cost_{ORC} = \left(C_{evp} + C_{con} + C_{exp} + C_p\right) \times k_c \tag{9}$$

where k_c is a multiplying factor of 1.2 that takes into account the cost of the working fluid and the auxiliary components such as piping in the ORC system; C_{evp} and C_{con} are the cost of the evaporator and the cost of the condenser, respectively, which are calculated from the cost correlation of the plate heat exchanger in Table 8.

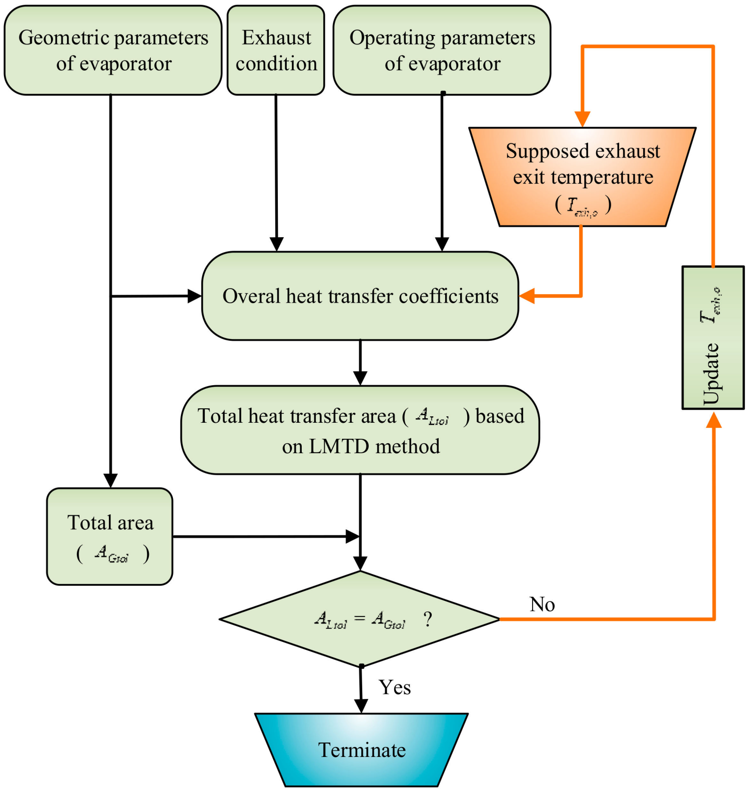

Figure 3. The flow chart of calculation for the heat exchanger (evaporator) model.

Meanwhile, the economic feasibility is usually taken into account when the ORC system is designed for the application, and the upfront cost always needs to be recovered as quickly as possible. The payback period of ORC installation on light-duty vehicles is further analyzed. Here, the payback period (PB) is defined as the ratio of the total investment cost to savings per year. For simplicity, the interest rate is neglected.

$$PB = \frac{Cost_{ORC}}{C_{sv}} \tag{10}$$

$$C_{sv} = LD \times FE \times FR \times C_{fuel} \tag{11}$$

where C_{sv} is the savings per year, LD is the average travel distance of the light-duty vehicle in a year, FE is the average fuel economy, is the potential fuel consumption reduction from the onboard ORC application, and C_{fuel} is the cost per liter of the fuel.

It is assumed that the average distance traveled by a light-duty vehicle is 500 km a day, and the vehicle works 255 days per year. Meanwhile, since the gasoline prices change rapidly because of crude oil supply, refinery operations, etc., and vary from country to country, the baseline gasoline price is assumed to be EUR 1.5/L according to the historical prices. The average fuel economy (FE) is approximately 5.6 L/100 km based on the EU 2015 emission regulation for light-duty passenger cars [38]. Since the fuel economy usually varies with the vehicle speed, the fuel economy can be further presented as a function of the vehicle speed and it is given by [42]

$$FE = \left(-0.21637 \times v_{\mathrm{km}} + 0.0013055 \times v_{\mathrm{km}}^2 + 0.24808 \times IRI + 13.3658\right) \times k_{fu} \tag{12}$$

where v_{km} is the vehicle speed (km/h), IRI is the international roughness index, and k_{fu} is a multiplying factor used for adjustment. The potential fuel consumption reduction (FR) usually refers to the relative fuel efficiency improvement [38], expressed by

$$FR = \frac{\dot{W}_{net}}{\dot{W}_E} \tag{13}$$

where $\dot{W}_E$ is the engine power.

3.4. Mass Model and Power Loss Correlations

It is reported in the literature that the mass of the ORC components can be evaluated based on the equipment parameters and manufacturer data. The correlations for the mass of the four main components in the ORC unit are presented in Table 9 [8,36]. The mass correlations of the expander and the pump depend, respectively, on the output power ($\dot{W}_{exp}$) and the power consumption ($\dot{W}_p$) while for plate heat exchangers, the mass correlation is based on the weight of exchanger auxiliary parts (M_{aux}) and the weight of a single heat transfer plate (M_{sp}) determined by the geometric parameters and the type of material. Details are referred to in Refs. [9,36].

Table 9. The mass correlations of the main ORC components.

Component	Correlation Equation
Expander	$M_{exp} = 0.3448\dot{W}_{exp} + 6.4655$
Heat exchanger	$M_{exch} = M_{aux} + N_p M_{sp}$
Pump	$M_p = 1.0746\dot{W}_p + 1.8022$

The total mass of the ORC unit is evaluated by the sum of the mass of the four main components and the mass of auxiliary parts in the system, such as the mass of control components, connecting pipes, and so on. The expression for the total mass of the ORC unit is presented:

$$M_{ORC} = \left(M_{evp} + M_{con} + M_{exp} + M_p\right) \times \delta \tag{14}$$

where δ is a coefficient that is adopted to take the mass of the auxiliary parts into account.

The increases in vehicle weight and the exhaust back pressure are two main drawbacks of installing the ORC unit on the exhaust pipe of a vehicle engine. Both of them lead to the decrease in engine performance. A correlation that evaluates the effect of extra weights on the increase of the engine load is presented by [8,36].

$$\dot{W}_{ORC,w} = \begin{cases} 0.04\dot{W}_{Eng}\frac{M_{ORC}}{0.1M_{vehicle}}, & sp > 47.2\ \text{km/h} \\ 0.06\dot{W}_{Eng}\frac{M_{ORC}}{0.1M_{vehicle}}, & sp \leq 47.2\ \text{km/h} \end{cases} \tag{15}$$

where sp is the vehicle speed, $\dot{W}_{Eng}$ is the ICE power, and $M_{vehicle}$ is the weight of the light-duty vehicle.

The extra power consumption of the engine comes from back pressure caused by the ORC unit. It is estimated by the following correlation [8,37]:

$$\dot{W}_{backp} = 0.02\dot{W}_{Eng}\frac{\Delta P_{bp}}{10} \tag{16}$$

where ΔP_{bp} is the total engine back pressure.

4. Optimization Results

4.1. The Thermoeconomic Optimization Results

The thermoeconomic optimization problem is carried out for four different working fluids (Table 2) to minimize SIC. Since the optimization problem is a mixed-integer non-linear programming (MINLP) problem, it is solved by the OPTI Toolbox integrated in the MATLAB software invoking the NOMAD solver. NOMAD is implemented based on the Mesh Adaptive Direct Search (MADS) algorithm, which can efficiently explore better solutions for a large spectrum of nonlinear problems [43]. The optimal system operating parameters and the geometric parameters of heat exchangers are simultaneously obtained in a solution corresponding to each working fluid.

The value of the optimization objectives, the total investment cost, and the corresponding optimized geometric parameters of the evaporator and the condenser are shown in Table 10. The working fluid RC490 achieves a minimum SIC of EUR 835.3/kW, which corresponds to the mean net output power of 3.19 kW and a total cost of EUR 2667.6. Different values of the optimization objective function are obtained using different working fluids. Under the investigated working fluids, it can be found that the lower SIC and higher mean net output power of ORC can be achieved using the organic working fluid with a higher critical temperature. This can be explained by the difference in heat absorption from the exhaust gas. The working fluid with a higher critical temperature can be heated to a higher temperature by the waste heat under the same evaporating pressure limit. Therefore, it can absorb more heat and generate more output power through the expander.

Table 10. The optimal geometric parameters and the values of objectives.

Working Fluid	Number of Evaporating Plates N_{pe}	Plate Length of Evaporator L_{pe} (m)	Number of Condensing Plates N_{pc}	Plate Length of Condenser L_{pc} (m)	SIC (EUR/kW)	Mean Net Output Power $\overline{\dot{W}_{net}}$ (kW)	Total Cost (EUR)
R245fa	57	0.40	45	0.60	1308.8	2.31	3023.4
R245ca	51	0.42	45	0.50	1080.5	2.59	2798.6
R601a	53	0.40	45	0.40	962.5	2.76	2652.9
RC490	49	0.45	45	0.40	835.3	3.19	2667.6

Table 11 shows the ORC operating parameters corresponding to each engine operating point of different working fluids obtained by the optimization. Generally, the optimal evaporating pressures are about 2500 kPa, and the optimal condensing pressures are close to 300 kPa, corresponding to different engine operating points for all working fluids except for the engine operating point 1, when R245fa is taken as working fluid. The pressure values of 300 kPa and 2500 kPa are the minimum and maximum values, respectively, in the optimized range. High evaporation pressure and low condensation pressure are good choices for all the working fluids to obtain high system performance. The condensing pressure (482.63 kPa) obtained for the cycle with working fluid R245fa at operating point 1 of the vehicle engine is higher because the exit temperature of the exhaust gas needs to be maintained within the constraint. Since the exhaust heat energy that enters the evaporator is low at operating point 1, the temperature of the working fluid at the evaporator inlet needs to be increased by increasing the condensing pressure to reduce the temperature difference between the working fluid and exhaust gas in the evaporator and to meet the temperature constraint of the exhaust.

Table 11. The optimal ORC operating parameters.

Engine Operating Point	**1**	**2**	**3**	**4**	**5**
Exhaust mass flow rate (g/s)	25.9	43.0	59.7	71.9	92.4
Exhaust temperature (°C)	595.1	716.7	779.2	800.7	804.1
R245fa					
Evaporating pressure (kPa)	2499.9	2500	2500	2500	2500
Superheat (°C)	19.75	20.62	20.59	18.81	20.09
Condensing pressure (kPa)	482.63	300	326.06	341.81	363.3
Subcooling (°C)	2	2	2	2	2
R245ca					
Evaporating pressure (kPa)	2500	2499.9	2500	2500	2500
Superheat (°C)	10.78	9.68	9.03	6.99	7.57
Condensing pressure (kPa)	300	300	300	300	300
Subcooling (°C)	2	2	2	2	2
R601a					
Evaporating pressure (kPa)	2500	2500	2500	2499.9	2500
Superheat (°C)	3.59	2.34	2.11	2.05	2.01
Condensing pressure (kPa)	300	300	300	300	300
Subcooling (°C)	2	2	2	2	2
RC490					
Evaporating pressure (kPa)	2499.9	2500	2500	2500	2500
Superheat (°C)	2.11	2.03	2	2	2
Condensing pressure (kPa)	300	300	300	300	300
Subcooling (°C)	2	2	2	2	2

It can be found that the small value of subcooling is preferred for all the working fluids while the optimal superheat for each working fluid is different. The optimal values of superheat vary while the exhaust condition (i.e., mass flow rate and temperature of exhaust) changes, which is particularly obvious for working fluids R245ca. Lowering the value of subcooling is good for reducing the heat dissipation requirement of the condenser, thereby helping to reduce the size of the condenser and its investment cost, and lowering subcooling also helps decrease the power consumed by the cooling fan. On the other hand, a higher superheat helps increase the output power of the expander by allowing the working fluid to absorb more exhaust heat. However, the larger size of the heat exchanger is required to increase the superheat value with the limitation of the low heat transfer coefficient. It increases the evaporator weight and cost, and, since the heat dissipation requirement of the working fluid with higher superheat increases after expansion, it would result in the increase of cooling consumption for the working fluid condensation to a set subcooling value. Hence, the optimal superheat is the result of a trade-off among factors such as the power output of the expander, cooling power consumption, and the ORC cost with SIC, which is taken as an objective function.

The system parameters after optimization are presented in Table 12. It can be found that the system constraints, such as the temperatures of working fluid at the evaporator outlet and the exit temperatures of the exhaust corresponding to each engine operating point, are all satisfied. The total weight of the ORC system obtained by optimization is in the range of 104 kg~117 kg. The changes of the total weight depend on the working fluid. In addition, the maximum average performance of the engine improved by the ORC system is 7.3%, achieved by RC490, and the minimum average engine performance improved is 5.2% when the R245fa is adopted.

Table 12. The parameters of the ORC system after optimization.

Engine Operating Point	1	2	3	4	5
The power of engine (kW)	13.0	26.4	37.2	44.1	54.4
R245fa					
Exhaust temperature at outlet (°C)	130.01	154.90	182.49	198.49	220.83
Temperature of the working fluid at evaporator outlet (°C)	153.13	154.00	154.00	152.20	153.51
Pressure drop at exhaust side (kPa)	0.97	2.73	5.28	7. 60	12.25
Mass flow rate of the working fluid (g/s)	53.39	99.09	149.50	185.80	232.60
The cooling air mass flow rate (kg/s)	0.31	2.05	3.13	3.89	4.86
The mass of ORC (kg)	116.27	116.27	116.27	116.27	116.27
Net output power (kW)	0.47	1.21	2.28	2.58	2.72
Engine performance improved by the ORC (%)	3.61	4.58	6.13	5.85	5.01
Payback period (year)			4.81		
R245ca					
Exhaust temperature at outlet (°C)	130.01	160.82	186.47	201.57	222.87
Temperature of the working fluid at evaporator outlet (°C)	159.50	158.40	157.75	155.71	156.29
Pressure drop at exhaust side (kPa)	1.13	3.16	6.10	8.78	14.12
Mass flow rate of working fluid (g/s)	48.92	99.30	148.93	184.44	229.62
The cooling air mass flow rate (kg/s)	0.42	1.11	2.11	3.01	4.63
The mass of ORC (kg)	109.43	109.43	109.43	109.43	109.43
Net output power (kW)	0.73	1.35	2.51	2.88	3.06
Engine performance improved by the ORC (%)	5.62	5.11	6.74	6.53	5.63
Payback period (year)			3.90		
R601a					
Exhaust temperature at outlet (°C)	138.67	169.97	196.22	212.32	233.58
Temperature of the working fluid at evaporator outlet (°C)	171.41	170.16	169.93	169.87	169.83
Pressure drop at exhaust side (kPa)	1.08	3.01	5.81	8.36	13.42
Mass flow rate of working fluid (g/s)	26.6	54.4	81.3	99.3	124.1
The cooling air mass flow rate (kg/s)	0.35	0.95	1.82	2.60	4.02
The mass of ORC (kg)	104.54	104.54	104.54	104.54	104.54
Net output power (kW)	0.77	1.44	2.63	3.04	3.29
Engine performance improved by the ORC (%)	5.92	5.45	7.07	6.89	6.05
Payback period (year)			3.44		
RC490					
Exhaust temperature at outlet (°C)	157.03	184.33	207.80	222.48	242.31
Temperature of the working fluid at evaporator outlet (°C)	198.29	198.21	198.18	198.18	198.18
Pressure drop at exhaust side (kPa)	1.30	3.61	6.93	9.96	16.01
Mass flow rate of working fluid (g/s)	24.2	49.7	74.7	91.4	114.4
The cooling air mass flow rate (kg/s)	0.19	0.45	0.79	1.05	1.47
The mass of ORC (kg)	105.42	105.42	105.42	105.42	105.42
Net output power (kW)	0.84	1.64	2.98	3.49	3.88
Engine performance improved by the ORC (%)	6.46	6.21	8.01	7.91	7.13
Payback period (year)			3.01		

Figure 4 shows the component costs for the ORC system with each working fluid. In this low-capacity ORC system (expander power output less than 9 kW and net power output less than 4 kW), the heat exchangers (i.e., the evaporator and the condenser) contribute the most, about 60% of the total cost of the system. This is similar to a 2 kW ORC system in Ref. [44], where 62% of the total costs were attributed to the heat exchangers. Since there are system constraints, the total cost of the onboard ORC using different working fluids only varies on a small scale after optimization. The cycle with R245fa costs the most (EUR 3023.4) and the minimum cost is the cycle with R601a (EUR 2652.9). However, the shortest payback period achieved by RC490 is 3.01 years when the ORC system has the highest net output power.

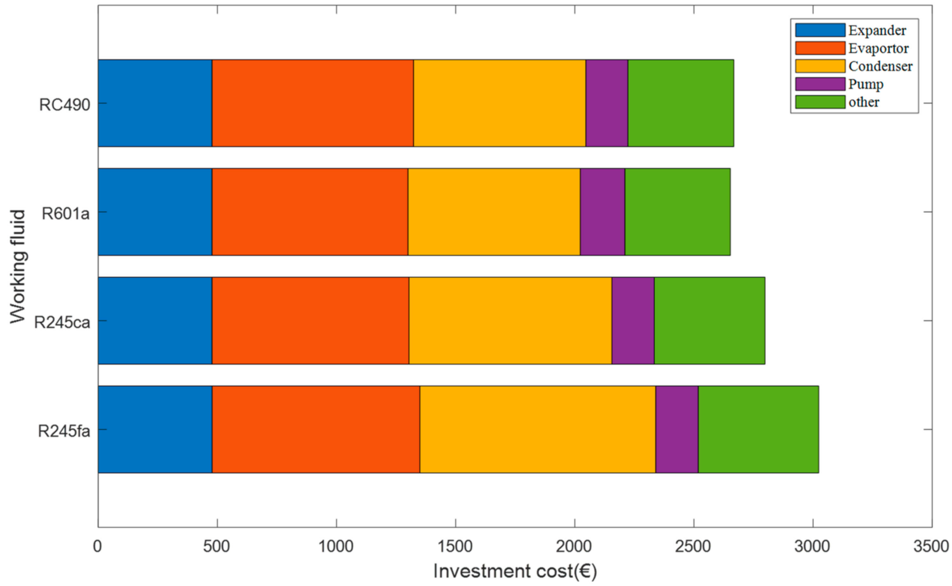

Figure 4. The component costs for ORC using different working fluids.

The power losses in the ORC system are demonstrated in Figure 5. It can be found that, for all the working fluids, the power loss caused by the added ORC weight is the maximum power loss at each engine operating point. The other power losses, caused, respectively, by back pressure, pumps, and fans, increase as the engine changes from a low-speed operating point to a higher speed operating point. The ratios of the power loss resulting from ORC mass and back pressure to the power produced by the expander at each operating point of the engine are presented in Table 13. Because of the negative impacts, the power loss accounts for a large part of the output power of the expander. Therefore, it is very important to account for the negative impacts of ORC weight and back pressure during the preliminary optimization design. This finding is consistent with the results of Ref. [36].

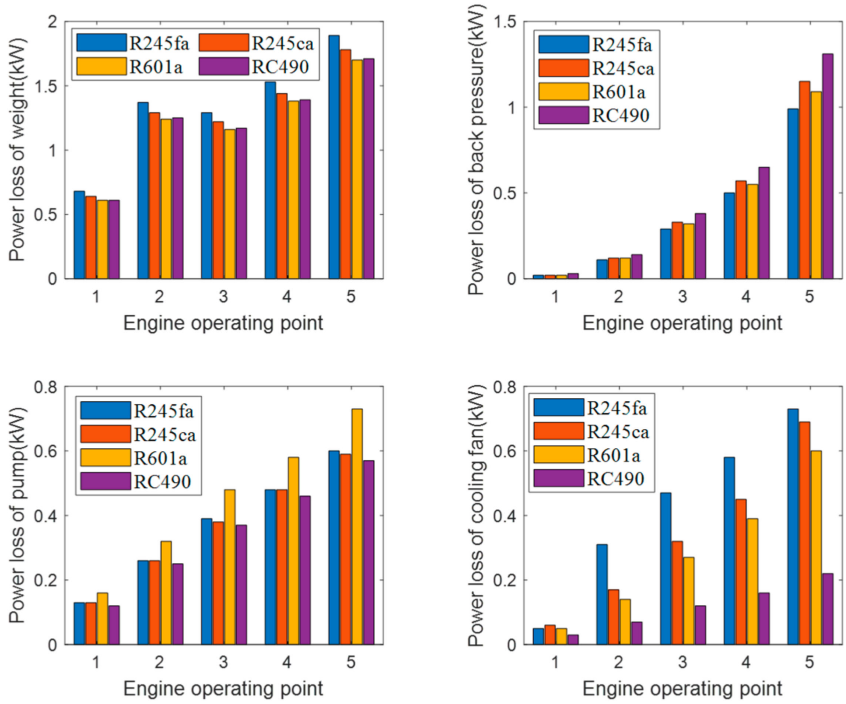

Figure 5. The power losses for ORC using different working fluids.

Table 13. Ratios of power loss to the expander power output.

	Ratios (%)				
Operating Point	**1**	**2**	**3**	**4**	**5**
R245fa	51.8	45.4	33.5	35.8	41.6
R245ca	41.8	44.2	32.6	34.5	40.3
R601a	51.6	55.7	45.8	48.8	55.6
RC490	48.3	50.9	40.6	43.2	49.5

4.2. *Off-Design Performance*

To test the off-design performance of the optimized onboard ORC, the ORC system is operated on 12 off-design exhaust conditions. These off-design exhaust conditions are generated by the Latin hypercube sampling method in the main interval of exhaust gas $T_{exh}[595\ldots804]^{\circ}\mathrm{C} \times \dot{m}_{exh}[25.9\ldots92.5]$ g/s (Figure 6).

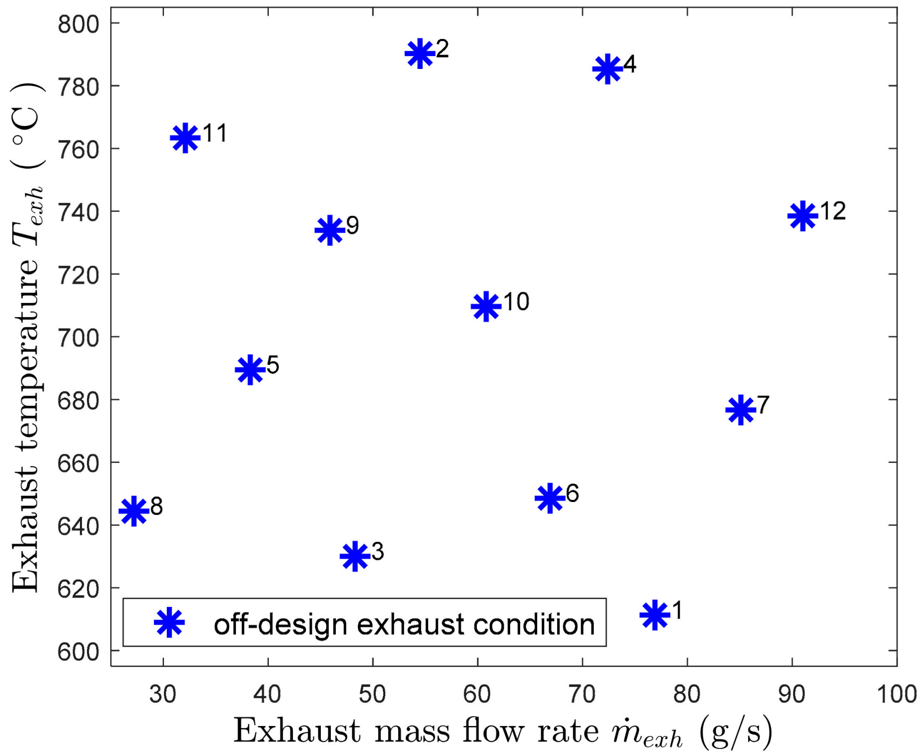

Figure 6. The off-design exhaust conditions.

For each exhaust condition in Figure 6, the working fluid flow in the cycle is adjusted through an optimization algorithm, such as sequential quadratic programming (SQP), to obtain the maximum net output power of the ORC system on the basis of the optimum geometric parameters of the evaporator and the condenser obtained by the thermoeconomic optimization. Figure 7 shows the results of the operation in the off-design exhaust conditions. The red double-dash line is the upper bound of the temperature of each working fluid at the evaporator outlet, and the red dotted line is the lower bound of the exhaust exit temperature after recovery. It can be found that both the constraints related to the exit temperature of exhaust gas and the temperature of the working fluid at the outlet of the evaporator can be satisfied in the off-design exhaust conditions while the positive net output powers are generated. This reflects the advantages of the design method based on multiple main exhaust conditions and avoids the infeasibility of ORC operation in off-design exhaust conditions, and ensures continuity and reliability of the practical operation of the onboard ORC.

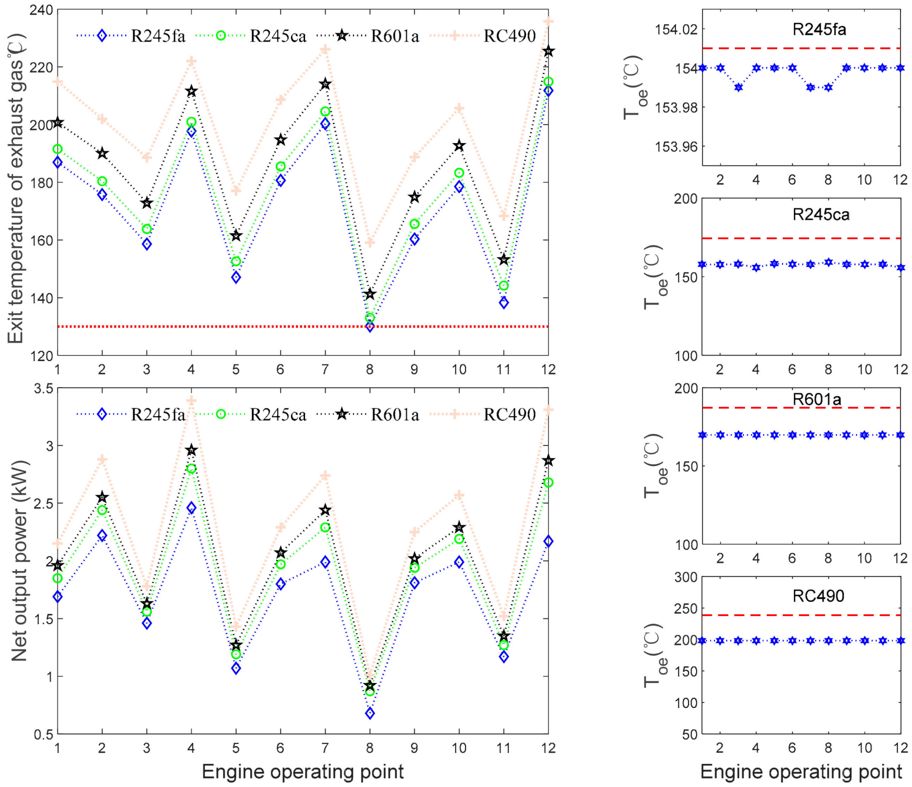

Figure 7. The net output powers and temperature constraints in off-design exhaust conditions.

4.3. Comparison with the Optimal Design, Taking the Net Output Power as an Objective Function

To show the benefits and effectiveness of the proposed design methodology through thermal–economic optimization, a comparison between the proposed method (named Design A) and an optimal design, taking the average ORC net output power as an objective function (named Design B), is carried out. The objective function of the average net output power is expressed as

$$\overline{\dot{W}}_{net} = \sum_{i=1}^{N_{ex}} w_i \dot{W}_{net,i} \tag{17}$$

For simplicity, only the optimization results of the ORC system with R245fa (i.e., the working fluid) are presented. Table 14 shows the objective function values resulting from the optimization of each design method. Though the higher average net output power is achieved by Design B, the comparison between the economics of the design result and the result of Design A decreases with an increase of the SIC from EUR 1308.8/kW to EUR 1382.5/kW and the payback period extended from 4.81 years to 5.13 years.

Table 14. The values of optimization functions for different design methods with R245fa.

Design Strategies	Objective	Payback Period (PB)
Design with SIC as an objective and the negative effects are considered (Design A)	$SIC = 1308.8$ (EUR/kW) $\left(\overline{\dot{W}}_{net} = 2.31 \text{ kW}\right)$	PB = 4.81 (year)
Design with $\overline{\dot{W}}_{net}$ as an objective and the negative effects are considered (Design B)	$\overline{\dot{W}}_{net} = 2.33$ (kW)(SIC= 1382.5 EUR/kW)	PB = 5.13 (year)
Design with SIC as an objective function but the negative effects are not considered (Design C)	$SIC = 594.35$ (EUR/kW) $\left(\overline{\dot{W}}_{net}= 4.32 \text{ kW}\right)$	PB = 2.17 (year)

4.4. Comparison with the Design without Taking the Negative Effects into Account

To demonstrate the importance of taking the negative effects during the onboard ORC thermoeconomic optimization, a comparison between the proposed optimal design method (Design A) and a thermoeconomic optimization without considering the negative effects caused by ORC weight and back pressure (named Design C) was also made. In Table 14, Design C has much higher average net out power ($\overline{\dot{W}}^{*}_{net}$= 4.32 kW) and much lower specific investment cost than Design A; this leads to a very short payback period (2.17 years). However, in practical applications, vehicle exhaust heat is recovered by ORC, and the practical issues, such as the weight added to the vehicle and back pressure, always exist. The influence of the practical aspects on the ORC performance, in fact, is significant (Table 13). Therefore, the performance of Design C needs to be re-evaluated in the presence of the negative effects on the basis of the optimization result obtained by Design C. Table 15 shows the verified results of Design C. It is found that a significant reduction is involved in the average net power out of cycle from 4.32 kW to 1.07 kW and the SIC increases from EUR 594.35/kW to EUR 2411.95/kW, and the payback period rapidly increases to 7.38 years, so it is less economical. Hence, it is not reasonable that Design C takes SIC as an objective function without considering the negative effects.

Table 15. Verification for Design C considering negative effects.

Operating Point Design C	**1**	**2**	**3**	**4**	**5**
Exhaust temperature at outlet (°C)	130.21	159.83	188.50	204.61	222.92
Working fluid temperature at the evaporator outlet (°C)	152.44	153.70	153.93	151.46	153.76
Net output power (kW)	0.59	1.09	1.71	1.53	0.48
Average net output power (kW)			1.07		
Specific investment cost (EUR/kW)			2411.95		
Payback period (year)			7.38		

Additionally, the optimal operating parameters (i.e., condensing pressure, evaporating pressure, subcooling, and superheat) obtained, respectively, by Design A, Design B, and Design C are presented in Figure 8. The top blue dash-dot line is the upper bound of the evaporating pressure and the bottom black dash-dot line is the lower bound of the condensing pressure. The carmine dash line is the lower bound of the superheat and subcooling. It is found that the optimal operating parameters from each design method are all within the set range and the optimal values of the operating parameters are very close. This illustrates that the system's optimal operation depends on the characteristics of the system itself and has nothing to do with the optimization goal.

4.5. Sensitivity Analysis of Payback Period

In addition to being affected by the thermodynamic characteristic of the cycle and the cost of the components, the economic indicators savings per year (C_{sv}) and the payback period (PB) are also subject to uncertainty due to the estimation of the average travel distance in a year and the fuel price. To know the vehicle's daily travel distance and the number of days worked each year influencing fuel prices, PBs for four different working fluids are given in Figures 9–11, respectively. Taking into account different intensities of vehicle use between countries, regions, and vehicle users, Figure 9 shows PB changes with the daily travel distance increased from 400 km to 700 km when the number of days worked each year is 255 days. Figure 10 shows PB changes with the number of working days each year increased from 240 to 285 when the vehicle's daily travel distance is 500 km. It is found in Figures 9 and 10 that, for each working fluid, a reduction is involved in the PB value with the increase in the travel distance or working days for the ORC designed from thermoeconomic optimization. In Figure 11, PBs become smaller when the fuel price varies from EUR 1/L to EUR 2/L. Therefore, it can be concluded that both the fuel price and the intensity of vehicle use (the daily travel distance and the number of working days each year) are critical parameters for ORC system payback estimation. The higher fuel price and higher intensity of vehicle use are good for achieving a small payback period, and it is possible to obtain a reasonable payback period (e.g., 3 years) when the working fluids with higher critical temperatures, such as RC490, are used in the onboard ORC system optimized by the proposed method.

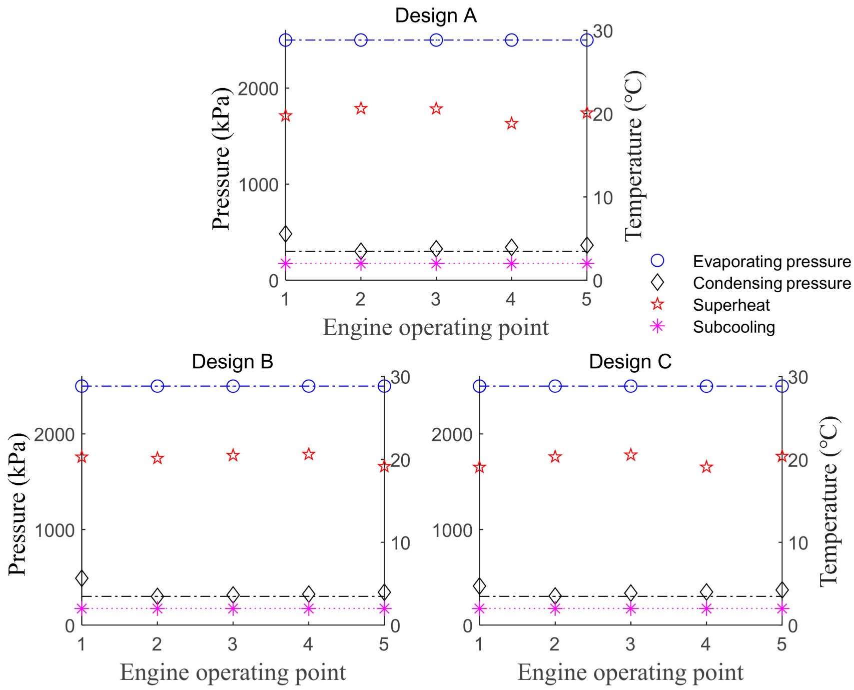

Figure 8. The optimal operating parameters of each design method.

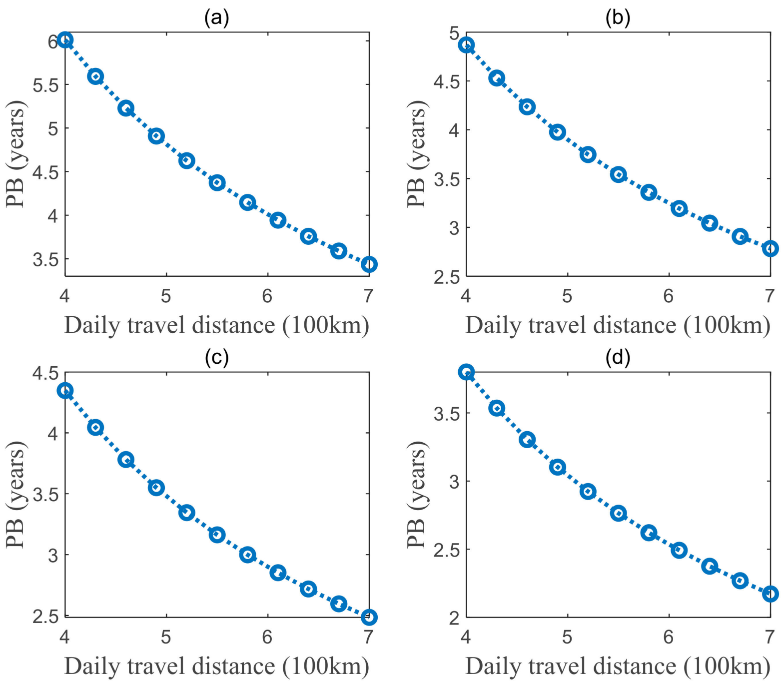

Figure 9. Evolution of the payback period (PB) vs. daily travel distance when the vehicle works for 255 days each year, fuel price is EUR 1.5/L, and the working fluid is (**a**) R245fa, (**b**) R245ca, (**c**) R601a, and (**d**) RC490, respectively.

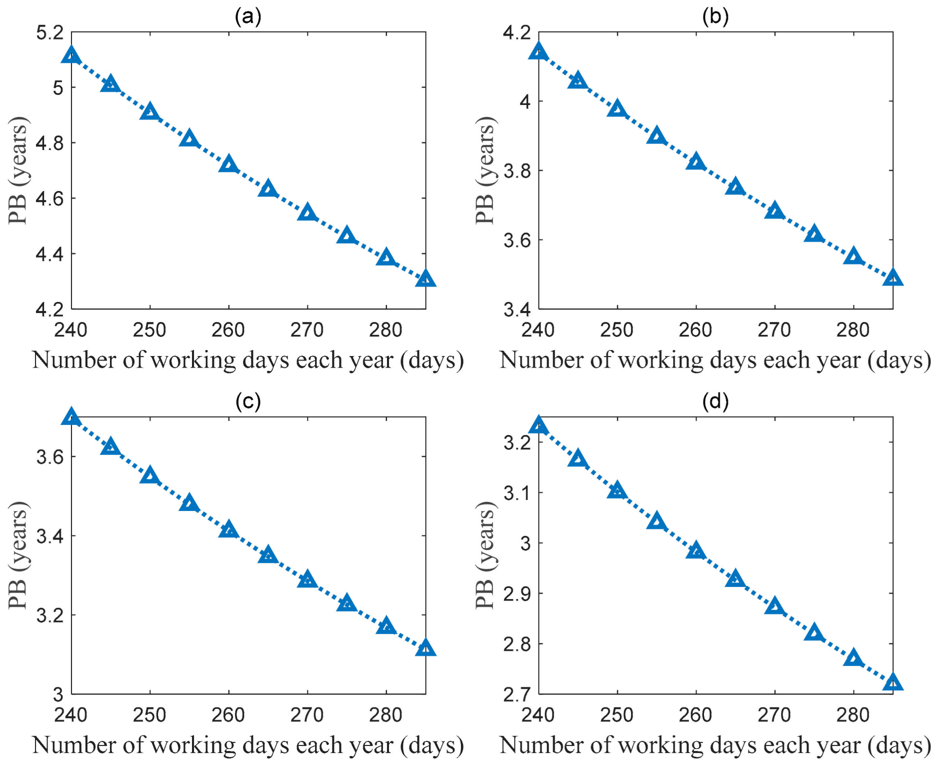

Figure 10. Evolution of the payback period (PB) vs. the number of working days each year when the daily travel distance is 500 km, fuel price is EUR 1.5/L, and the working fluid is (**a**) R245fa, (**b**) R245ca, (**c**) R601a, and (**d**) RC490, respectively.

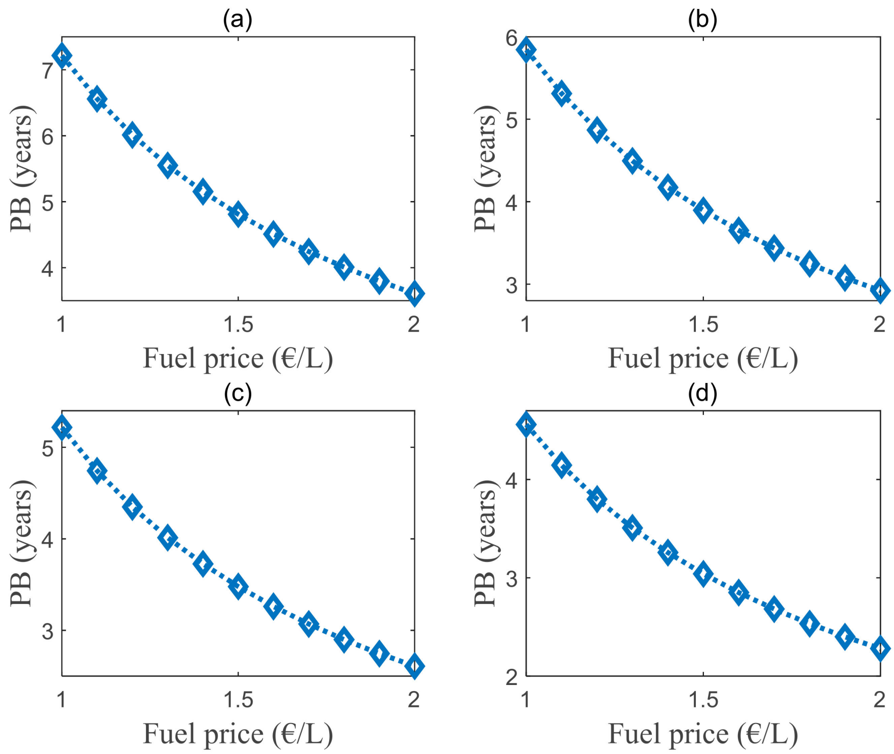

Figure 11. Evolution of the payback period (PB) vs. the fuel price when the daily travel distance is 500 km, the number of working days each year is 255, and the working fluid is (**a**) R245fa, (**b**) R245ca, (**c**) R601a, and (**d**) RC490, respectively.

5. Conclusions

A thermoeconomic optimization model for an onboard ORC is presented in this paper. A cost-effective ORC with high thermodynamic performance is designed to recover the exhaust heat of a light-duty vehicle. The negative effects of the vehicle-mounted ORC are considered in the optimization model for practical applications. The optimization design is performed for four different working fluids to minimize the thermoeconomic index (SIC) so that the maximum net output power can be obtained and the investment cost can be minimized. The geometric parameters and operating parameters are simultaneously obtained through solving the optimization problem with the NOMAD algorithm, which applies to the mixed-integer nonlinear programming (MINLP) problem. A comparison between the proposed design method and the design method without taking the negative effects into account is discussed. Moreover, a comparison between the proposed method and the design with mean net output power as an optimization objective is also carried out. The comparison results show the advantages of the proposed method for the onboard ORC system design. The major results and conclusions can be summarized as follows:

1. A comprehensive design method of the ORC system for exhaust heat recovery of a light-duty vehicle using thermoeconomic optimization is proposed, and the most cost-effective solution is provided.
2. Among the investigated working fluids, the design using the organic working fluid with a higher critical temperature can achieve lower SIC, higher average net output power, and a shorter payback period. The shortest payback time, by RC490 with the highest critical temperature, is 3.01 years in this study.
3. The thermoeconomic optimizations with different objectives are compared, indicating that design with SIC as an objective function is more beneficial than the design with net output power, and the effect of the working fluid on the net output power of the cycle is greater than its impact on the total investment cost of the cycle.
4. To achieve a cost-effective ORC design, the negative effects of the vehicle-mounted ORC are considered.
5. The optimal values of superheat for the onboard ORC system are different, depending on the different working fluids and exhaust gas conditions.

In practice, the exhaust gas condition varies with the vehicle speed changes and road conditions. Therefore, control is needed in practical applications. The control design will also affect the design result; consequently, a thermoeconomic optimization considering the control effects is worthy of study in the future. In addition, the optimal ORC structure may be different under different heat source conditions (e.g., temperature). At the same time, the category of working fluid will also affect the efficiency of the ORC system. Therefore, exploring the performance of ORCs with different structures and fluids is an important research direction, and this issue will also be further explored in future work.

Author Contributions: Conceptualization, X.W. and N.Z.; methodology, X.W. and J.C.; software, N.Z.; validation, L.X., S.L. and W.C.; formal analysis, W.C.; investigation, L.X.; resources, S.L.; data curation, N.Z.; writing—original draft preparation, X.W.; writing—review and editing, J.C.; supervision, J.C. and L.X.; project administration, S.L.; funding acquisition, S.L. and W.C. All authors have read and agreed to the published version of the manuscript.

Funding: This research was funded by Natural Science Foundation of Huzhou, China, grant number 2021YZ05; the Open Research Project of the State Key Laboratory of Industrial Control Technology, Zhejiang University, China, grant number ICT2021B40; the In-novation Team by Department of Education of Guangdong Province, China, grant number 2020KCXTD041; Public Welfare Technology Application and Research Projects of Zhejiang Province, China grant number LGG22F030016.

Institutional Review Board Statement: Not applicable.

Informed Consent Statement: Not applicable.

Data Availability Statement: Not applicable.

Conflicts of Interest: The authors declare no conflict of interest.

Nomenclature

ρ	Density (kg/m^3)	$\dot{W}$	Power
T	Temperature (K)	A	Heat transfer area (m^2)
$\dot{m}$	Mass flow rate (kg/s)	η	Efficiency
$\dot{Q}$	Quantity of heat	C	Cost
P	Pressure (kpa)	L	Length (m)
D	Diameter (m)	M	Weight (kg)
U	Total heat transfer coef.	SH	Superheat (K)
TV	Total volume	TM	Total mass
h	Enthalpy (kJ/kg)	SC	Subcooling
ICE	Internal combustion engine	SIC	Specific investment cost
OP	Operating parameters	GP	Geometric parameters
VC	Volume coefficient	TIC	Total investment cost
PB	Payback period	W	Width
ORC	Organic Rankine cycle	V	Volume
Superscripts		-	Nominal or mean value
Subscripts			
f	Fluid/friction	exh	Exhaust gas
evp/e	Evaporator	o	Outer
c/con	Condenser	A	Air fan
pl	partial	in	Inlet
w	Exchanger wall	p	Pump/plate/port
Eng	Engine	bp	Back pressure
yr	Year	is	Isotropy
exp	Expander	liq/l	Liquid
e	Exergy/evaporator	$exch$	Exchanger
eff	Effective	tp	Two phases
d	Discharge		

References

1. Colonna, P.; Casati, E.; Trapp, C.; Mathijssen, T.; Larjola, J.; Turunen-Saaresti, T.; Uusitalo, A. Organic Rankine Cycle Power Systems: From the Concept to Current Technology, Applications, and an Outlook to the Future. *J. Eng. Gas Turbines Power* **2015**, *137*, 100801. [CrossRef]
2. Chintala, V.; Kumar, S.; Pandey, J.K. A technical review on waste heat recovery from compression ignition engines using organic Rankine cycle. *Renew. Sustain. Energy Rev.* **2018**, *81*, 493–509. [CrossRef]
3. Wang, T.; Zhang, Y.; Zhang, J.; Shu, G.; Peng, Z. Analysis of recoverable exhaust energy from a light-duty gasoline engine. *Appl. Therm. Eng.* **2013**, *53*, 414–419. [CrossRef]
4. Vázquez, J.; Sanz-Bobi, M.A.; Palacios, R.; Arenas, A. State of the art of thermoelectric generators based on heat recovered from the exhaust gases of automobiles. In Proceedings of the 7th European Workshop on Thermoelectrics, Pamplona, Spain, 3–4 October 2002.
5. Aghaali, H.; Ångström, H.-E. A review of turbocompounding as a waste heat recovery system for internal combustion engines. *Renew. Sustain. Energy Rev.* **2015**, *49*, 813–824. [CrossRef]
6. Oyewunmi, O.A.; Kirmse, C.J.; Haslam, A.J.; Müller, E.A.; Markides, C.N. Working-fluid selection and performance investigation of a two-phase single-reciprocating-piston heat-conversion engine. *Appl. Energy* **2017**, *186*, 376–395. [CrossRef]
7. Saidur, R.; Rezaei, M.; Muzammil, W.; Hassan, M.; Paria, S.; Hasanuzzaman, M. Technologies to recover exhaust heat from internal combustion engines. *Renew. Sustain. Energy Rev.* **2012**, *16*, 5649–5659. [CrossRef]
8. Wu, X.; Chen, J.; Xie, L. Optimal design of organic Rankine cycles for exhaust heat recovery from light-duty vehicles in view of various exhaust gas conditions and negative aspects of mobile vehicles. *Appl. Therm. Eng.* **2020**, *179*, 115645. [CrossRef]
9. Imran, M.; Haglind, F.; Lemort, V.; Meroni, A. Optimization of organic rankine cycle power systems for waste heat recovery on heavy-duty vehicles considering the performance, cost, mass and volume of the system. *Energy* **2019**, *180*, 229–241. [CrossRef]
10. Yebi, A.; Xu, B.; Liu, X.; Shutty, J.; Anschel, P.; Filipi, Z.; Onori, S.; Hoffman, M. Estimation and predictive control of a parallel evaporator diesel engine waste heat recovery system. *IEEE Trans. Control Syst. Technol.* **2017**, *27*, 282–295. [CrossRef]
11. Rahbar, K.; Mahmoud, S.; Al-Dadah, R.K.; Moazami, N.; Mirhadizadeh, S.A. Review of organic Rankine cycle for small-scale applications. *Energy Convers. Manag.* **2017**, *134*, 135–155. [CrossRef]

12. He, S.; Chang, H.; Zhang, X.; Shu, S.; Chen, D. Working fluid selection for an Organic Rankine Cycle utilizing high and low temperature energy of an LNG engine. *Appl. Therm. Eng.* **2015**, *90*, 579–589. [CrossRef]
13. Lecompte, S.; Huisseune, H.; van den Broek, M.; Vanslambrouck, B.; De Paepe, M. Review of organic Rankine cycle (ORC) architectures for waste heat recovery. *Renew. Sustain. Energy Rev.* **2015**, *47*, 448–461. [CrossRef]
14. Zhang, W.; Wang, E.; Meng, F.; Zhang, F.; Zhao, C. Closed-loop PI control of an Organic Rankine Cycle for engine exhaust heat recovery. *Energies* **2020**, *13*, 3817. [CrossRef]
15. Valencia, G.; Fontalvo, A.; Forero, J.D. Optimization of waste heat recovery in internal combustion engine using a dual-loop organic Rankine cycle: Thermo-economic and environmental footprint analysis. *Appl. Therm. Eng.* **2021**, *182*, 116109. [CrossRef]
16. Li, J.; Yang, Z.; Hu, S.; Yang, F.; Duan, Y. Thermo-economic analyses and evaluations of small-scale dual-pressure evaporation organic Rankine cycle system using pure fluids. *Energy* **2020**, *206*, 118217. [CrossRef]
17. Ping, X.; Yao, B.; Zhang, H.; Yang, F. Thermodynamic, economic, and environmental analysis and multi-objective optimization of a dual loop organic Rankine cycle for CNG engine waste heat recovery. *Appl. Therm. Eng.* **2021**, *193*, 116980. [CrossRef]
18. Yang, F.; Zhang, H.; Song, S.; Bei, C.; Wang, H.; Wang, E. Thermoeconomic multi-objective optimization of an organic Rankine cycle for exhaust waste heat recovery of a diesel engine. *Energy* **2015**, *93*, 2208–2228. [CrossRef]
19. Wang, Z.; Hu, Y.; Xia, X.; Zuo, Q.; Zhao, B.; Li, Z. Thermo-economic selection criteria of working fluid used in dual-loop ORC for engine waste heat recovery by multi-objective optimization. *Energy* **2020**, *197*, 117053. [CrossRef]
20. Amicabile, S.; Lee, J.-I.; Kum, D. A comprehensive design methodology of organic Rankine cycles for the waste heat recovery of automotive heavy-duty diesel engines. *Appl. Therm. Eng.* **2015**, *87*, 574–585. [CrossRef]
21. Galindo, J.; Climent, H.; Dolz, V.; Royo-Pascual, L. Multi-objective optimization of a bottoming Organic Rankine Cycle (ORC) of gasoline engine using swash-plate expander. *Energy Convers. Manag.* **2016**, *126*, 1054–1065. [CrossRef]
22. Hajabdollahi, Z.; Hajabdollahi, F.; Tehrani, M.; Hajabdollahi, H. Thermo-economic environmental optimization of Organic Rankine Cycle for diesel waste heat recovery. *Energy* **2013**, *63*, 142–151. [CrossRef]
23. Sanaye, S.; Khakpaay, N. Thermo-economic multi-objective optimization of an innovative cascaded organic Rankine cycle heat recovery and power generation system integrated with gas engine and ice thermal energy storage. *J. Energy Storage* **2020**, *32*, 101697. [CrossRef]
24. Yang, F.; Cho, H.; Zhang, H.; Zhang, J. Thermoeconomic multi-objective optimization of a dual loop organic Rankine cycle (ORC) for CNG engine waste heat recovery. *Appl. Energy* **2017**, *205*, 1100–1118. [CrossRef]
25. Guillaume, L.; Lemort, V. Comparison of different ORC typologies for heavy-duty trucks by means of a thermo-economic optimization. *Energy* **2019**, *182*, 706–728. [CrossRef]
26. Serafino, A.; Obert, B.; Vergé, L.; Cinnella, P. Robust optimization of an organic Rankine cycle for geothermal application. *Renew. Energy* **2020**, *161*, 1120–1129. [CrossRef]
27. Yang, F.; Cho, H.; Zhang, H.; Zhang, J.; Wu, Y. Artificial neural network (ANN) based prediction and optimization of an organic Rankine cycle (ORC) for diesel engine waste heat recovery. *Energy Convers. Manag.* **2018**, *164*, 15–26. [CrossRef]
28. Yang, C.; Xie, H.; Zhou, S.K. Overall optimization of Rankine cycle system for waste heat recovery of heavy-duty vehicle diesel engines considering the cooling power consumption. *Sci. China Technol. Sci.* **2015**, *59*, 309–321. [CrossRef]
29. Quoilin, S.; Broek, M.V.D.; Declaye, S.; Dewallef, P.; Lemort, V. Techno-economic survey of Organic Rankine Cycle (ORC) systems. *Renew. Sustain. Energy Rev.* **2013**, *22*, 168–186. [CrossRef]
30. Yang, S.-C.; Hung, T.-C.; Feng, Y.-Q.; Wu, C.-J.; Wong, K.-W.; Huang, K.-C. Experimental investigation on a 3 kW organic Rankine cycle for low-grade waste heat under different operation parameters. *Appl. Therm. Eng.* **2017**, *113*, 756–764. [CrossRef]
31. Tocci, L.; Pal, T.; Pesmazoglou, I.; Franchetti, B. Small scale Organic Rankine Cycle (ORC): A techno-economic review. *Energies* **2017**, *10*, 413. [CrossRef]
32. Raghulnath, D.; Saravanan, K.; Mahendran, J.; Lakshmanan, P. Analysis and optimization of organic Rankine cycle for IC engine waste heat recovery system. *Mater. Today Proc.* **2020**, *21*, 30–35. [CrossRef]
33. Hoang, A.T. Waste heat recovery from diesel engines based on Organic Rankine Cycle. *Appl. Energy* **2018**, *231*, 138–166. [CrossRef]
34. Groniewsky, A.; Wagner, C. Investigation of the Effect of the Regenerative Heat Exchanger on the Performance of Organic Rankine Cycles Using Perturbed Chain–Statistical Associating Fluid Theory Equation of State. *Ind. Eng. Chem. Res.* **2020**, *59*, 19643–19656. [CrossRef]
35. Lion, S.; Michos, C.N.; Vlaskos, I.; Rouaud, C.; Taccani, R. A review of waste heat recovery and Organic Rankine Cycles (ORC) in on-off highway vehicle Heavy Duty Diesel Engine applications. *Renew. Sustain. Energy Rev.* **2017**, *79*, 691–708. [CrossRef]
36. Usman, M.; Imran, M.; Yang, Y.; Park, B.S. Impact of organic Rankine cycle system installation on light duty vehicle considering both positive and negative aspects. *Energy Convers. Manag.* **2016**, *112*, 382–394. [CrossRef]
37. ALEŠ, H. Waste heat recovery using ORC for bottoming IC engine. In Proceedings of the Conference on Exploitation of Waste Heat Potentials in Europe Dubrovnik, Dubrovnik, Croatia, 5 October 2017; pp. 2–13.
38. Upendra, K.; Grauers, A. *Synergy and Conflicts between Waste Heat Recovery System and Hybrid Electric Vehicle*; Chalmers University of Technology: Gothenburg, Sweden, 2015.
39. Hsieh, Y.; Lin, T. Saturated flow boiling heat transfer and pressure drop of refrigerant R-410A in a vertical plate heat exchanger. *Int. J. Heat Mass Transf.* **2002**, *45*, 1033–1044. [CrossRef]

40. Lecompte, S.; Huisseune, H.; van den Broek, M.; De Schampheleire, S.; De Paepe, M. Part load based thermo-economic optimization of the Organic Rankine Cycle (ORC) applied to a combined heat and power (CHP) system. *Appl. Energy* **2013**, *111*, 871–881. [CrossRef]
41. Kuo, W.; Lie, Y.; Hsieh, Y.; Lin, T. Condensation heat transfer and pressure drop of refrigerant R-410A flow in a vertical plate heat exchanger. *Int. J. Heat Mass Transf.* **2005**, *48*, 5205–5220. [CrossRef]
42. Wang, L.; Ji, H.; Wang, H. Research on Driving Speed Range Based on Optimum Carbon Emission and Fuel Consumption Optimization. *Transp. Energy Conserv. Environ. Prot.* **2020**, *16*, 8–12.
43. Le Digabel, S. Algorithm 909: NOMAD: Nonlinear optimization with the MADS algorithm. *ACM Trans. Math. Softw. (TOMS)* **2011**, *37*, 1–15. [CrossRef]
44. Tchanche, B.F.; Quoilin, S.; Declaye, S.; Papadakis, G.; Lemort, V. Economic feasibility study of a small scale organic rankine cycle system in waste heat recovery application. In Proceedings of the Engineering Systems Design and Analysis, Istanbul, Turkey, 12–14 July 2010; pp. 249–256.